NASA TECHNICAL NOTE

NASA TN D-2478

NASA TN D-2478

EXPERIMENTAL RESULTS OF COOLING A 12.5° SEMIVERTEX ANGLE CONE BY EJECTION OF HYDROGEN AND HELIUM FROM ITS APEX AT MACH 7

by George F. Klich and Edward W. Leyhe

Langley Research Center
Langley Station, Hampton, Va.

NATIONAL AERONAUTICS AND SPACE ADMINISTRATION • WASHINGTON, D. C. • SEPTEMBER 1964

EXPERIMENTAL RESULTS OF COOLING A 12.5° SEMIVERTEX ANGLE CONE BY EJECTION OF HYDROGEN AND HELIUM FROM ITS APEX AT MACH 7

By George F. Klich and Edward W. Leyhe

Langley Research Center
Langley Station, Hampton, Va.

NATIONAL AERONAUTICS AND SPACE ADMINISTRATION

For sale by the Office of Technical Services, Department of Commerce,
Washington, D.C. 20230 -- Price $1.00

EXPERIMENTAL RESULTS OF COOLING A 12.5° SEMIVERTEX ANGLE CONE BY EJECTION OF HYDROGEN AND HELIUM FROM ITS APEX AT MACH 7

By George F. Klich and Edward W. Leyhe
Langley Research Center

SUMMARY

An experimental study has been made of the problem of cooling a 12.5° semivertex angle cone having a 2-inch (5.08-cm) base diameter by ejection of a coolant from its apex. Two coolants, hydrogen and helium gases, were investigated for a range of coolant-flow rates with the cone at zero angle of attack. The experimental studies were carried out in the 7-inch (17.8-cm) Mach 7 pilot tunnel at the Langley Research Center at a stream stagnation temperature of about 3600° R (2000° K) with stream Reynolds numbers ranging from about 0.45×10^6 to 1.20×10^6 per foot (1.48×10^6 to 3.95×10^6 per m).

The addition of a coolant affected heat-transfer characteristics of the boundary layer such that local film heat-transfer coefficients with coolant flow were higher than those with no coolant flow. Large reductions in local recovery temperatures were effected by injection of relatively small quantities of the coolant gases into the boundary layer of the cone. By use of measured equilibrium wall temperatures with coolant flow and a modified correlating parameter, all data from both coolants were correlated with the exception of cases where unstable coolant injection was noted. The correlation clearly defines the thermal protection afforded the cone by steady upstream coolant ejection for the conditions investigated.

INTRODUCTION

Manned hypersonic flight within the earth's atmosphere will require sophisticated thermal-protection systems for vehicle protection in order that aerodynamic shapes may be maintained. One method of thermal protection which appears promising for manned hypersonic vehicles is cooling by mass addition. A number of reports have been published regarding this mode of thermal protection. Most of these reports (refs. 1 and 2, for example) have treated a transpired stagnation point region. A few of them have attempted to explore the downstream cooling afforded either by transpiration at the nose or leading edge (ref. 3) or by coolant injection from slots (ref. 4). However, thermal-protection processes of these latter cooling modes are more complicated than pure transpiration cooling inasmuch as mixing becomes an important part of the process. At the

present time there is a very limited amount of published experimental data with which empirical or theoretical analyses can be developed regarding downstream cooling effectiveness, particularly for test conditions simulating hypersonic flight. Hence the present investigation was undertaken and the results and analyses are presented herein.

An investigation was conducted during which hydrogen and helium gases were used as coolants to protect a 12.5° semivertex angle cone subjected to aerodynamic heating at Mach 7. The coolant gases were ejected in an upstream direction through an orifice at the apex of the cone. The total energy level of the test stream used was about 1200 Btu/lb (2790 kJ/kg). Stream stagnation temperatures were about 3600° R (2000° K), and the resulting stream Reynolds numbers ranged from about 0.45×10^6 to 1.2×10^6 per foot (1.48×10^6 to 3.95×10^6 per m).

SYMBOLS

Units applicable to the physical quantities defined in this section are given both in the U.S. Customary Units and in the International System of Units (SI). Relationships between the two systems for the units used in this report are given in the appendix.

C_p	specific heat at constant pressure, Btu/lb-°R (J/kg-°K)
D	diameter, in. (m)
F	nondimensional parameter, $\frac{w_c/S}{(\rho V)_l}$
h	film heat-transfer coefficient, Btu/ft^2-sec-°R (W/m^2-°K)
l	length, ft (m)
M	Mach number
m	exponent
N_{Pr}	Prandtl number
N_{Re}	Reynolds number, 1/ft (1/m)
N_{St}	Stanton number
n	exponent
p	pressure, psia (N/m^2)

r	radius, in. (m)
S	area cooled, ft^2 (m^2)
T	temperature, ^oR (^oK)
t	time, sec (s)
V	velocity, ft/sec (m/s)
w	mass flow rate, lb/sec (kg/s)
x	distance from apex of cone to TC station, ft (m)
z	exponent
μ	absolute viscosity, lb/ft-sec (Ns/m^2)
ρ	density, lb/ft^3 (kg/m^3)
τ	thickness, ft (m)
Φ	circumferential location of thermocouple, deg

Subscripts:

aw	adiabatic wall
b	base of model
c	coolant
ℓ	local conditions outside boundary layer
o	without coolant flow
r	recovery temperature
s	main stream behind normal shock
t	stagnation condition behind normal shock
w	wall
∞	free stream

MODELS, APPARATUS AND TESTS

Models

The basic model shape used in the present tests was a 12.5° semivertex angle cone having a 2-inch-(5.08-cm) diameter base and a removable tip section (fig. 1). Interchangeable tips included a solid tip with a 0.125-inch-(3.17-mm) radius spherical-section nose for the reference or no coolant flow conditions (fig. 1(a)), and two frustrum sections, in which the small-diameter end was a coolant discharge orifice. The diameters of the orifices were 0.199 inch (5.05 mm) and 0.100 inch (2.54 mm) (fig. 1(b)). The major components of the model were fabricated from 347 stainless steel. The heat-transfer surface was the portion of the cone between stations at x/l of 0.252 and 0.965. This section of the conical shell was machined to a wall thickness of 0.0115 inch (0.292 mm). It was supported at the forward end by a boron nitride insulator and at the rear by a teflon insulator in an attempt to minimize heat loss by conduction. The surface was instrumented with 19 no. 36 chromel-alumel wire thermocouples spotwelded to the inside surface. The longitudinal and circumferential locations of the thermocouples are indicated by the table in figure 1(b). Individual thermocouples were made up by spotwelding two wires to the surface approximately 0.02 inch (0.508 mm) apart in a plane perpendicular to the axis of the cone. For the case where the cone was cooled, the coolant was introduced through the base of the cone into a plenum chamber from which it was discharged through the orifice at the apex. Hence, coolant discharge was always along the axis of the cone in an upstream direction.

Pertinent details and dimensions for the configurations tested are shown as figure 1. Photographs of the configurations are shown as figure 2.

Coolant System

The apparatus for supplying coolant gases to the model is shown schematically in figure 3. The coolant gas was supplied from high-pressure storage bottles. The rate of coolant flow was controlled by pressure-regulating valves in conjunction with observation of the indicator on a rotameter flow meter. The valves were adjusted to maintain a predetermined setting on the flow meter. Actual flow rates were established from flow-meter calibration curves with the known readings and the measured gas line pressure and temperature upstream of the meter.

The three-way valve located between the storage bottles and the flow meter (fig. 3) permitted helium to be utilized as a purge for the system (as well as a coolant for the model) whenever hydrogen was used as a coolant. After the tunnel was started, and immediately before any hydrogen was allowed to flow, the system was purged with helium. Upon completion of the test and before tunnel shutdown, helium was used to clear the system of all hydrogen gas that remained in the cooling system or tunnel test section.

Test Facility

The facility used to conduct the tests was the 7-inch (17.8-cm) Mach 7 pilot tunnel at the Langley Research Center. This facility is a blowdown tunnel which achieves high energy level flows by the combustion of a hydrocarbon fuel in air under pressure. The resulting combustion products are expanded through the nozzle and used as the test medium. Downstream of the test section the flow passes through a diffuser and is pumped to the atmosphere by a single-stage annular air ejector.

The Mach 7 nozzle has an exit diameter of 7.5 inches (19.1 cm). Calibrations of the flow in the test region have indicated a usable test core of 2.5 to 3.0 inches (6.3 to 7.6 cm) in diameter, dependent upon pressure and temperature. Over this core the total temperature varies approximately 2 percent and the normal shock-pressure ratio varies approximately 2 percent. During the present investigation, both methane (CH_4) and ethylene (C_2H_4) gases were used as fuels in the tunnel. However, the use of different fuels did not affect the results obtained.

Test Procedure

Tests were conducted at tunnel stagnation pressures of approximately 600, 1000, and 1500 psia (4.13, 6.89, and 10.33 kN/m^2) and at a stagnation temperature near 3600° R (2000° K). The resulting free-stream Reynolds number varied between 0.45×10^6 and 1.20×10^6 per foot (1.48×10^6 and 3.95×10^6 per m). The models were kept out of the stream until test conditions were established, then quickly inserted into the test region. The time required for insertion was approximately 1/4 second. The average test interval was about 25 seconds for the cooled model and about 3 seconds for the uncooled model. The models were extracted from the stream prior to tunnel shutdown.

For the case of the cooled model, coolant flow was established prior to insertion of the model into the test region. Hence, the models entered the stream with a fixed coolant flow rate. Tests were conducted with four different coolant mass flow rates for each coolant at each stagnation pressure.

Outputs from the various pressure transducers and thermocouples connected to model apparatus and tunnel were generally recorded as continuous traces by means of oscillographs. However, in some cases the outputs were recorded by a central data recording system which recorded the output from each measuring device twenty times each second during the test interval.

In addition to outputs from thermocouples and pressure transducers, schlieren photographs of the flow field near the cone were taken. The pictures were made with a camera having a 1/50-second shutter speed and a continuous light source.

Data Reduction

Temperature histories and pressures were determined from the recordings of the outputs from thermocouples and pressure transducers. Local film heat-transfer coefficients along the heat-transfer surface were determined from the temperature histories by assuming one-dimensional heat flow in the thin wall such that:

$$h = \frac{\rho_w C_{p,w} \tau_w \frac{dT_w}{dt}}{(T_{aw} - T_w)} \tag{1}$$

In performing these computations the adiabatic wall temperature T_{aw} was defined as

$$T_{aw} = \sqrt{N_{Pr}}(T_t - T_l) + T_l \tag{2}$$

since the Reynolds number, based on the length of the model, was sufficiently low to insure laminar boundary layers on the models. The Prandtl number, as well as the total and static temperatures, were derived for the combustion-products test medium according to reference 5.

A typical plot of $\frac{dT_w}{dt}$ as a function of the parameter $(T_{aw} - T_w)$ for the uncooled cone is presented in figure 4. For the ideal case of no heat loss due to radiation or conduction, the conditions under which the one-dimensional equation for film heat-transfer coefficient is valid, $\frac{dT_w}{dt}$ must go to zero as $(T_{aw} - T_w)$ goes to zero. In the real case, for the uncooled model in a high-energy stream, the assumed conditions are not met throughout the test interval. During the initial temperature rise, there is a lag as heat flux is established in the metal wall followed by a time interval where the assumed conditions are met. (The duration of this interval is dependent upon local heating rate and wall thickness.) There is then a final interval during which the assumed conditions are not met because the surface may be radiating and/or conduction may be significant. In reducing the data, the slope of the $\frac{dT_w}{dt}$ plotted against $(T_{aw} - T_w)$ curve was taken as the slope of a line passing through the origin and tangent to the experimental data curve (fig. 4).

From the data obtained, there was evidence of heat leakage through the insulating gasket at the downstream end of the heat-transfer surface. As a consequence, the data obtained from thermocouples at stations $x/l = 0.834$, 0.888, and 0.902 were considered unusable and are not presented. Also, very little data were obtained from station $x/l = 0.283$ because of thermocouple failure shortly after the investigation commenced.

During the test intervals, cone-surface temperatures were not permitted to exceed 1500° R (834° K) in order to avoid thermal distortion of the thin conical surface. For cases with coolant flow, equilibrium temperatures were controlled

by the coolant; therefore, test runs were made long enough to insure that equilibrium temperatures were actually measured. A typical plot of surface temperatures along the cone as a function of time during a test interval is presented in figure 5. The measured equilibrium surface temperature was considered to be the local recovery temperature for heat transfer with coolant flow. Local film heat-transfer coefficients were then computed by use of equation (1).

The maximum possible errors in the data presented are believed to be as indicated in the following table. In general, however, it is believed that the accuracies are better than those indicated.

Quantity	Maximum error, percent
Local temperature	3
Total temperature	2
Total pressure	5
Coolant-flow rate	4
Local film heat-transfer coefficient	5

RESULTS AND DISCUSSION

Cone without Coolant

The experimentally determined distribution of film heat-transfer coefficients along an element of the uncooled heat-transfer surface is presented in figure 6. Distributions for the three different test stream Reynolds numbers are presented. It is noted that the data are reduced to a single distribution by dividing local values of the heat-transfer coefficient by the square root of the stream Reynolds number. This reduction is as would be expected for laminar flow. Also presented is the theoretical distribution of laminar film heat-transfer coefficients as derived from reference 6. Stagnation-point values for use in the theoretical distribution of reference 6 were calculated according to reference 7.

It is noted from figure 6 that the experimentally determined film heat-transfer coefficients fall above the theoretical values by an amount that is generally considered to be within the accuracy of the theory. More important is the indication that experimental scatter of the data is relatively small and that the trend of the experiment is in agreement with that of theory.

Cone with Coolant Ejection

It will be noted from figure 5 that with coolant flow, temperature changes with time and local recovery temperatures at the various temperature measurement stations varied greatly along the cone with coolant flow. It may also be noted that the equilibrium temperatures near the apex of the cone were lower than the initial wall temperatures. The lower equilibrium wall temperatures occurred with larger coolant flow rates even though the coolant stagnation temperature was about the same as the initial wall temperature. In such cases, apparently very

little mixing had been achieved near the surface and the heat transfer in that region was governed largely by the recovery temperature of the coolant.

The measured local recovery temperatures were used with equation (1) to derive the local film heat-transfer coefficients. Results typical of all data are shown in figure 7. In this figure, ratios of measured local film heat-transfer coefficients with coolant flow to those without coolant flow are presented as a function of coolant flow rate for the various temperature measurement stations. For the particular pressure shown, there are no data presented for the thermocouple stations at x/l of 0.455 with a coolant flow rate of 9.09×10^{-4} lb/sec (4.12×10^{-4} kg/s) as there was very little change in model wall temperature at that particular thermocouple station during the test interval. Consequently, for that station, the film heat-transfer coefficient was indeterminate from equation (1).

It is shown in figure 7 that the heat-transfer coefficients for the cases with coolant flow were higher than those obtained without coolant flow by at least a factor of 2. The increase in the heat-transfer coefficient is a result of the coolant flow causing not only large reductions in the local recovery temperature but also significant changes in local boundary-layer characteristics such as temperature gradients and transport properties. In addition, the distribution of the film heat-transfer coefficient, because of the above-mentioned coolant effects, depends upon the interaction of a mixing wake with an initial coolant boundary-layer growth. This distribution would be expected to be complicated and this contention is borne out by a close examination of figure 7. Thus, it did not appear that any simple procedure for correlating all the data would be developed. For the present data at least, the film heat-transfer coefficient was considered to be an unsatisfactory measure of coolant effectiveness.

As was noted in the previous paragraph, the reduction in recovery temperature is the primary advantage of cooling by film injection. Since the recovery temperature distributions were smooth and monotonic, equilibrium conditions appeared more promising than the transient conditions for determining coolant effectiveness. For equilibrium conditions, the coolant effectiveness is often represented by a so-called coolant effectiveness parameter defined as $\left(\frac{T_r - T_c}{T_{aw} - T_c}\right)$ (see ref. 8, for example). However, it remains to relate this effectiveness parameter to physical quantities important in describing the flow pattern.

When thermal equilibrium is reached, there is zero net heat flow to the wall. The only energy transfer is between the stream and coolant. This energy transfer is a function of many complex factors such as the total enthalpy difference between the stream and coolant and gradients produced by mixing. The magnitudes and distribution of these various factors are dependent upon the geometry of the body being cooled and the method of injection. For example, in the present case of cooling a cone by the injection of a coolant at the apex, all of the coolant passes through a single orifice. As a consequence, the effective body shape of the model with coolant flow is vastly different from that of the uncooled cone. Changes in the effective shape of the model are illustrated in figure 8 which presents schlieren photographs taken with different flow rates of hydrogen gas as the coolant at a model stagnation pressure of 5.8 psia

(40.0 kN/m^2). The interface between the coolant and the main stream in figure 8(a), which is with a coolant flow rate of 2.99×10^{-4} lb/sec (1.36×10^{-4} kg/s), indicates only a slight change in the effective shape of the cone. However, in figure 8(b) which is with a coolant flow rate of 9.10×10^{-4} lb/sec (4.13×10^{-4} kg/s), the effective shape of the model appears to be a hemisphere-cylinder-cone with a cylinder diameter over twice the diameter of the injection orifice with a change in the cone angle from that of the actual model.

The preceding may not be the case if the coolant were injected with a uniform distribution along the cone length. The local coolant mean temperature and concentration in the boundary layer would also be different for the two methods of coolant injection. If the body shape were changed from three dimensional to two dimensional, the "effectiveness" of a given coolant injected into the boundary layer by a particular method would also change.

It is thus clear that care must be exercised when assumptions are made concerning the effects of coolant injection on boundary-layer flow and heat-transfer characteristics. It is likewise clear that no simple physically meaningful heat balance equation is yet available with which to determine a correlating parameter for the coolant effectiveness.

In order to find a useful correlating parameter, recourse was made to transpiration cooling practices. Transpiration cooling theory (see ref. 9) assumes that the coolant film is extremely thin with no mixing and no distortion of the local stream flow. The energy transferred by the stream appears only as heat absorbed by the coolant and, at a stagnation point, the coolant temperature is equal to the wall temperature. Data from transpiration cooled surfaces have been successfully correlated in references 9 and 10 by use of the parameter $\frac{w/S}{N_{St,o}(\rho_l V_l)} \frac{C_{p,c}}{C_{p,l}}$ $\left(\text{in ref. 9, } C_{p,c} = C_{p,l}\right)$. Furthermore, this parameter has been used with some success to define the downstream effectiveness of a coolant ejected upstream of a solid surface (for example, see refs. 3 and 10). As a result of this success, it was decided to examine the degree of correlation afforded by this parameter for the present data. Therefore, $\frac{T_r - T_c}{T_{aw} - T_c}$ was plotted as a function of $\frac{F}{N_{St,o}} \frac{C_{p,c}}{C_{p,l}}$ for the different test conditions and coolant ejection orifices, and are presented in figure 9. In the term $\frac{T_r - T_c}{T_{aw} - T_c}$, the coolant temperature T_c is the recovery temperature of the coolant in the boundary layer. In cases of large coolant flow rates where no effect of the main stream reaches the wall, the coolant recovery temperature determines, and is the lower limit for equilibrium wall temperatures. The local Stanton number, $N_{St,o}$ for the uncooled surface used in the correlating parameter is based on the experimentally determined film heat-transfer coefficients (fig. 6). The specific heats of hydrogen and helium were evaluated according to references 11 and 12.

It will be noted that the results obtained at a particular stagnation pressure form discrete curves dependent upon the coolant used or the apex orifice diameter used. In figure 9(a), which shows data from stagnation point pressure of 5.8 psia (40.0 kN/m^2) and the 0.199-inch-(5.05-mm) orifice, the data for hydrogen as the coolant are distinctly separated from those for helium as the coolant. In figure 9(b), which includes data from stagnation-point pressure of 8.9 psia (61.4 kN/m^2) and the 0.199-inch-(5.05-mm) coolant injection orifice, the data from the individual coolant gases are again separated. Figure 9(c) shows a noticeable separation of data obtained with the higher flow rates of hydrogen from the small (0.100-inch-(2.54-mm) diameter) coolant orifice at a stagnation-point pressure of 8.9 psia (61.4 kN/m^2). Similar flow-rate results are indicated in figure 9(d) which presents data from a stagnation-point pressure of 13.8 psia (95.2 kN/m^2), with the 0.199-inch-(5.05-mm) diameter coolant ejection orifice. In this case, there is also a separation or scatter in the data for helium as the coolant at the higher flow rates.

In attempting to analyze the aforementioned results, it was concluded that correlation of the data was not achieved partly because of the inadequacy of the parameter $\frac{F}{N_{St,o}} \frac{C_{p,c}}{C_{p,l}}$. It was believed that for the present method of coolant injection, mixing as well as the work done by the stream on the injected coolant must be accounted for. As a result, two additional factors indicative of these physical phenomena were included in the correlating parameter. One factor was $\frac{\rho_w \mu_w}{\rho_l \mu_l}$, which is a term that is common to most equations defining heat transfer and is an index to viscous effects and mixing which affect the efficiency of an injected coolant (see ref. 13). For coolant gases of like viscosities and equal molecular weights, the ratio $\frac{\rho_w \mu_w}{\rho_l \mu_l}$ can be reduced to a ratio of temperatures $\left(\frac{T_l}{T_w}\right)^z$. The other factor was a momentum ratio $\frac{\rho_c V_c^2}{\rho_s V_s^2}$, which is indicative of the work the stream must do to arrest the coolant flow in the upstream direction and accounts for changes in coolant injection velocity and direction. This second factor is associated with the deformation of shock-shapes and changes in stand-off distances as a result of coolant injection. The two factors were written in the form $\left(\frac{\rho_c \mu_c}{\rho_l \mu_l}\right)^m$ and $\left(\frac{\rho_c V_c^2}{\rho_s V_s^2}\right)^n$ and the exponents were evaluated from the experimental data.

It was found that most of the data obtained in the present investigation could be correlated with the parameter $\frac{F}{N_{St,o}} \frac{C_{p,c}}{C_{p,l}} \left(\frac{\rho_w \mu_w}{\rho_l \mu_l}\right)^{0.24} \left(\frac{\rho_c V_c^2}{\rho_s V_s^2}\right)^{0.2}$ where $\frac{\rho_c V^2}{\rho_s V_s^2}$ was evaluated as the ratio of the impulse of the coolant to that of the main stream behind a normal shock by assuming that the velocities of both gases

were zero at the interface. The term $\frac{\rho_w \mu_w}{\rho_l \mu_l}$ was evaluated at wall conditions for the coolant and at the outer edge of the boundary layer for the main stream.

Using this modified parameter, the data of figure 9 are replotted in figure 10. From inspection of figure 10, it is clear that the data correlate well for both coolants and all conditions with the exception of data in figure 10(c) and a portion of the data in figure 10(d). Figure 10(c) includes all data obtained with the 0.100-inch-(2.54-mm) diameter injection orifice at a stagnation pressure of 8.9 psia (61.4 kN/m^2). The excepted data of figure 10(d) are (1) from the largest flow rate of hydrogen and (2) from the largest flow rates of helium, all of which were obtained with the 0.199-inch (5.05-mm) orifice diameter at a stagnation pressure of 13.8 psia (95.2 kN/m^2). The curve through the data is the same for each part of figure 10, indicating that with the noted exceptions, all data could be correlated on one curve with the modified parameter.

Upon examination of schlieren data for the cases where correlation was not achieved, evidence was found of unsteady flow from the coolant orifice. Such unsteadiness was not noted for the cases where correlation was achieved. A typical series of schlieren photographs indicating the instability is presented in figure 11. As previously described, these photographs were taken with a 1/50-second exposure. Hence, the motion of the shock was not "stopped." The instability, when it occurred, appeared in the picture as a multiple-exposure of the bow shock. It is indicated that during the exposure, the shock moved within the observed limits. The reason for the observed instability of coolant flow is not understood. However, other investigators have observed similar fluctuations in the discharge of forward-facing jets immersed in hypersonic streams (see, for example, ref. 14).

The result of the instability on the effectiveness of the present method of cooling a cone is evidenced as an increase in equilibrium wall temperatures above those for steady flow for a particular coolant flow rate. It is obvious, therefore, that coolant flow instability of the type experienced is undesirable from the standpoint of thermal protection and is also not accounted for by the present correlating parameters.

A direct comparison of the thermal protection afforded by the two coolants investigated is made in figure 12. Here the coolant flow required to maintain a specific longitudinal location ($x/l = 0.780$) of the present 12.5° cone, at a given temperature from about 700° R (388° K), to about 1500° R (834° K), is indicated. Data from each of the coolants are presented for each pressure altitude simulated in the present tests. Coolant requirements are shown as a ratio of the coolant flow rate to the flow rate of the Mach 7 test stream through an area equivalent to that of the base of the model.

It may be noted from figure 12, that for the test configuration at the same altitude, flow rate requirements for gaseous helium are about twice the flow rate requirements for gaseous hydrogen to maintain the same reduced equilibrium wall temperature at the particular temperature measuring station. The smaller requirements for hydrogen are primarily due to its higher specific heat.

Although the curves of figure 12 represent data from the test configuration, extrapolation may be made to other 12.5° semivertex angle cones under similar flight conditions with proportional coolant ejection orifices provided consideration is given to changes in the film heat-transfer coefficients (no coolant flow) with distance from the tip of the cone.

The indicated shift in the curves for the 0.199-inch-(5.05-mm) diameter ejection orifice at 94,000-foot (28.7-km) pressure altitude and for the 0.100-inch-(2.54-mm) diameter orifice with hydrogen as the coolant at 105,000-foot (32-km) pressure altitude reflect the increase in coolant flow rate requirements to offset the flow instability previously noted.

In general, it will also be noted that for the zero angle-of-attack case studied in this investigation, very small quantities of coolant are required as a thermal protection for a 12.5° semivertex angle cone. Defining the effectiveness of similar cooling systems under angle-of-attack conditions and problems presented by the resulting crossflows are considerably more difficult than those encountered in the present limited investigation. The study of the effects of such crossflows on an injected coolant are subjects for further investigations.

CONCLUDING REMARKS

An experimental study has been made of the problem of cooling a 12.5° semivertex angle cone having a 2-inch (5.08-cm) base diameter by coolant ejection at its apex. Two coolants, hydrogen and helium, were investigated for a range of coolant flow rates and test stream Reynolds numbers. The experimental studies were carried out in the 7-inch (17.8-cm) Mach 7 pilot tunnel at the Langley Research Center at a stagnation temperature of about 3600° R (2000° K) for the cone at zero angle of attack.

The addition of a coolant affected heat-transfer characteristics of the boundary layer such that local film heat-transfer coefficients with coolant flow were higher than those with no coolant flow. Large reductions in local recovery temperatures were effected by injection of relatively small quantities of the coolant gases into the boundary layer of the cone. By the use of a modified correlating parameter, all data from both coolants were correlated with the exception of cases where unstable coolant injection was noted. The correlation clearly defines the thermal protection afforded by upstream coolant injection for the body geometry and conditions investigated with steady coolant flow.

Langley Research Center,
National Aeronautics and Space Administration,
Langley Station, Hampton, Va., June 17, 1964.

APPENDIX

CONVERSION OF U.S. CUSTOMARY UNITS TO SI UNITS

The International System of Units (SI) was adopted by the Eleventh General Conference on Weights and Measures, Paris, October 1960, in Resolution No. 12 (ref. 15). Conversion factors required for units used in this report are:

Physical quantity	U.S. customary unit	Conversion factor*	SI unit
Area	ft^2	9.290304×10^{-2}	meters^2 (m^2)
Density	lb/ft^3	16.018463	kilograms/meter^3 (kg/m^3)
Flow rate	lb/sec	0.453592	kilograms/second (kg/s)
Heat-transfer coefficient	$Btu/ft^2\text{-}^oR\text{-}sec$	2.042808×10^4	watts/meter^2-^{o}K ($W/m^2\ ^oK$)
Length	in.	0.0254	meters (m)
Pressure	psi	6.894757×10^3	newtons/meter^2 (N/m^2)
Specific heat	$Btu/lb\text{-}^oF$	4.184×10^3	joules/kilogram-degree Kelvin ($J/kg\text{-}^oK$)
Temperature	^oR	5/9	degrees Kelvin (^{o}K)
	(^{o}F + 459.67)	5/9	degrees Kelvin (^{o}K)
Thermal efficiency	Btu/lb	2.32444×10^3	joules/kilogram (J/kg)
Velocity	ft/sec	0.3048	meters/second (m/s)
Viscosity	lb/ft-sec	1.488164	newton-seconds/meter^2 (Ns/m^2)

*Multiply value given in U.S. customary unit by conversion factor to obtain equivalent value in SI unit.

Prefixes to indicate multiples of units are:

10^{-2} centi (c)
10^{-3} milli (m)
10^{3} kilo (k)
10^{6} mega (M)

REFERENCES

1. Roberts, Leonard: Mass Transfer Cooling Near the Stagnation Point. NASA TR R-8, 1959. (Supersedes NACA TN 4391.)

2. Johnson, B. V.; and Hartnett, J. P.: Heat Transfer From a Cylinder in Crossflow With Transpiration Cooling. J. Heat Transfer, vol. 85C, no. 2, May 1963, pp. 173-179.

3. Witte, William G.; and Rashis, Bernard: An Experimental Investigation and Correlation of the Heat Reduction to Nonporous Surfaces Behind a Porous Leading Edge Through Which Coolant is Ejected. NASA TM X-235, 1960.

4. Papell, S. Stephen: Effect on Gaseous Film Cooling of Coolant Injection through Angled Slots and Normal Holes. NASA TN D-299, 1960.

5. Leyhe, E. W.; and Howell, R. R.: Calculation Procedure for Thermodynamic, Transport, and Flow Properties of the Combustion Products of a Hydrocarbon Fuel Mixture Burned in Air with Results for Ethylene-Air and Methane-Air Mixtures. NASA TN D-914, 1962.

6. Lees, Lester: Laminar Heat Transfer Over Blunt-Nosed Bodies at Hypersonic Flight Speeds. Jet Propulsion, vol. 26, no. 4, 1956, pp. 259-269, 274.

7. Fay, J. A.; and Riddell, F. R.: Theory of Stagnation Point Heat Transfer in Dissociated Air. Jour. Aero. Sci., vol. 25, no. 2, Feb. 1958, pp. 73-85, 121.

8. Bartle, E. Roy; and Leadon, Bernard M.: The Effectiveness as a Universal Measure of Mass Transfer Cooling for a Turbulent Boundary Layer. Proc. Heat Transfer Fluid Mech. Inst., Stanford Univ. Press, 1962, pp. 27-41.

9. Rubesin, Morris W.: An Analytical Estimation of the Effect of Transpiration Cooling on the Heat-Transfer and Skin-Friction Characteristics of a Compressible, Turbulent Boundary Layer. NACA TN 3341, 1954.

10. Rashis, Bernard; and Hopko, Russell N.: An Analytical Investigation of Ablation. NASA TM X-300, 1960.

11. Hilsenrath, Joseph; Beckett, Charles W.; et al.: Tables of Thermal Properties of Gases. NBS Cir 564, U.S. Dept. Commerce, 1955.

12. Keyes, Frederick G.: The Heat Conductivity, Viscosity, Specific Heat, and Prandtl Number for Thirteen Gases. Project SQUID, Tech. Rep. No. 37, M.I.T., Apr. 1, 1952.

13. Lees, Lester: Convective Heat Transfer With Mass Addition and Chemical Reactions. Third AGARD Colloquium, M. W. Thring, O. Lutz, J. Fabri, and A. H. Lefebvre, eds., Pergamon Press, 1958, pp. 451-498.

14. Romeo, David J.; and Sterrett, James R.: Exploratory Investigation of the Effect of a Forward-Facing Jet on the Bow Shock of a Blunt Body in a Mach Number 6 Free Stream. NASA TN D-1605, 1963.

15. Anon.: International System of Units, Resolution No. 12. NASA TT F-200, 1964.

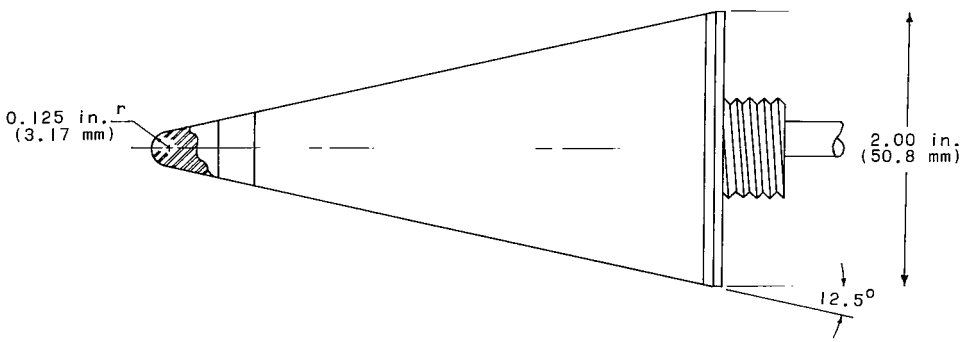

(a) Model with solid tip section.

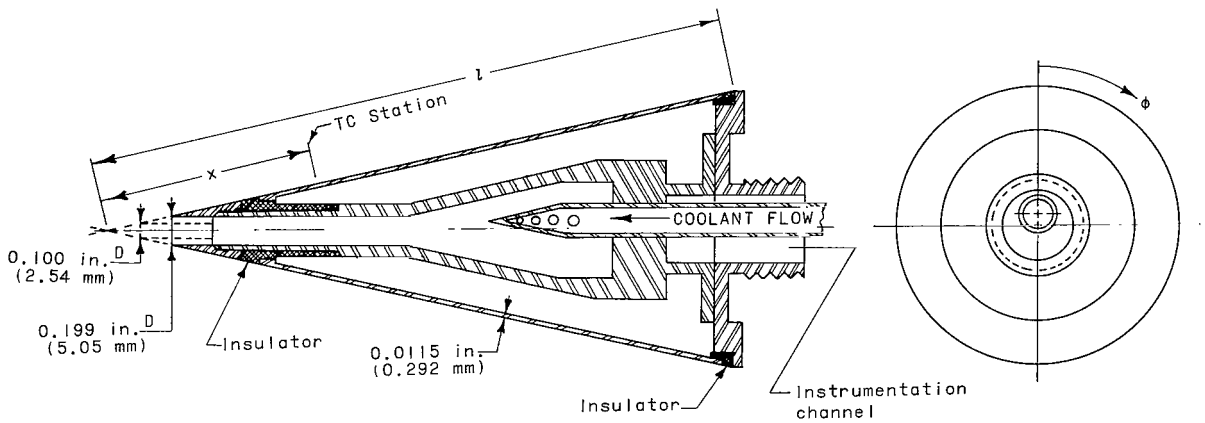

THERMOCOUPLE STATION		
x/l	TC Number	ϕ, deg
0.283	1	0
.347	2	0
.401	3	0
.455	4	0
.509	5	0
	14	90
	15	180
	16	270
.564	6	0
.618	7	0
.672	8	0
.726	9	0
.780	10	0
.834	11	0
.888	12	0
	17	90
	18	180
	19	270
.942	13	0

(b) Details of coolant ejection system in model and instrumentation of the heat-transfer surface.

Figure 1.- Sketch of model.

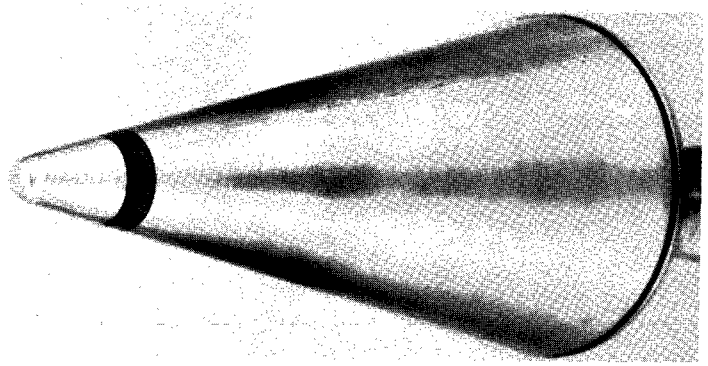

(a) Model with solid tip section. L-63-10144

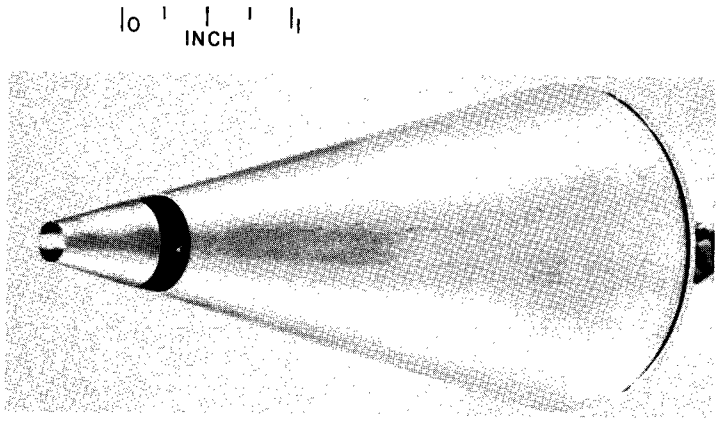

L-63-10143

(b) Model with 0.199-inch (5.05-mm) diameter coolant ejection orifice.

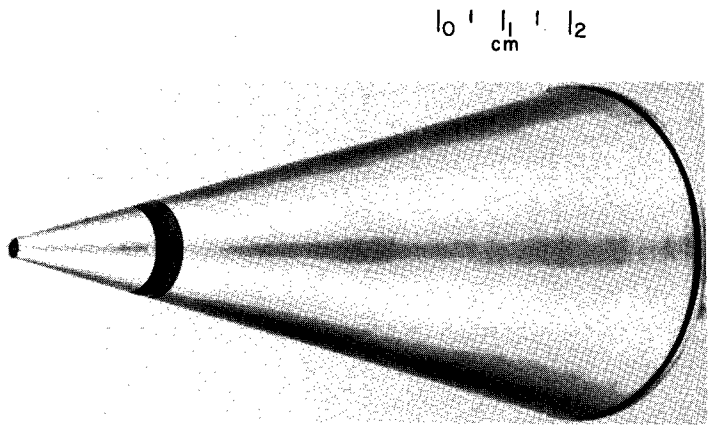

L-63-10142

(c) Model with 0.100-inch (2.54-mm) diameter coolant ejection orifice.

Figure 2.- Photographs of model.

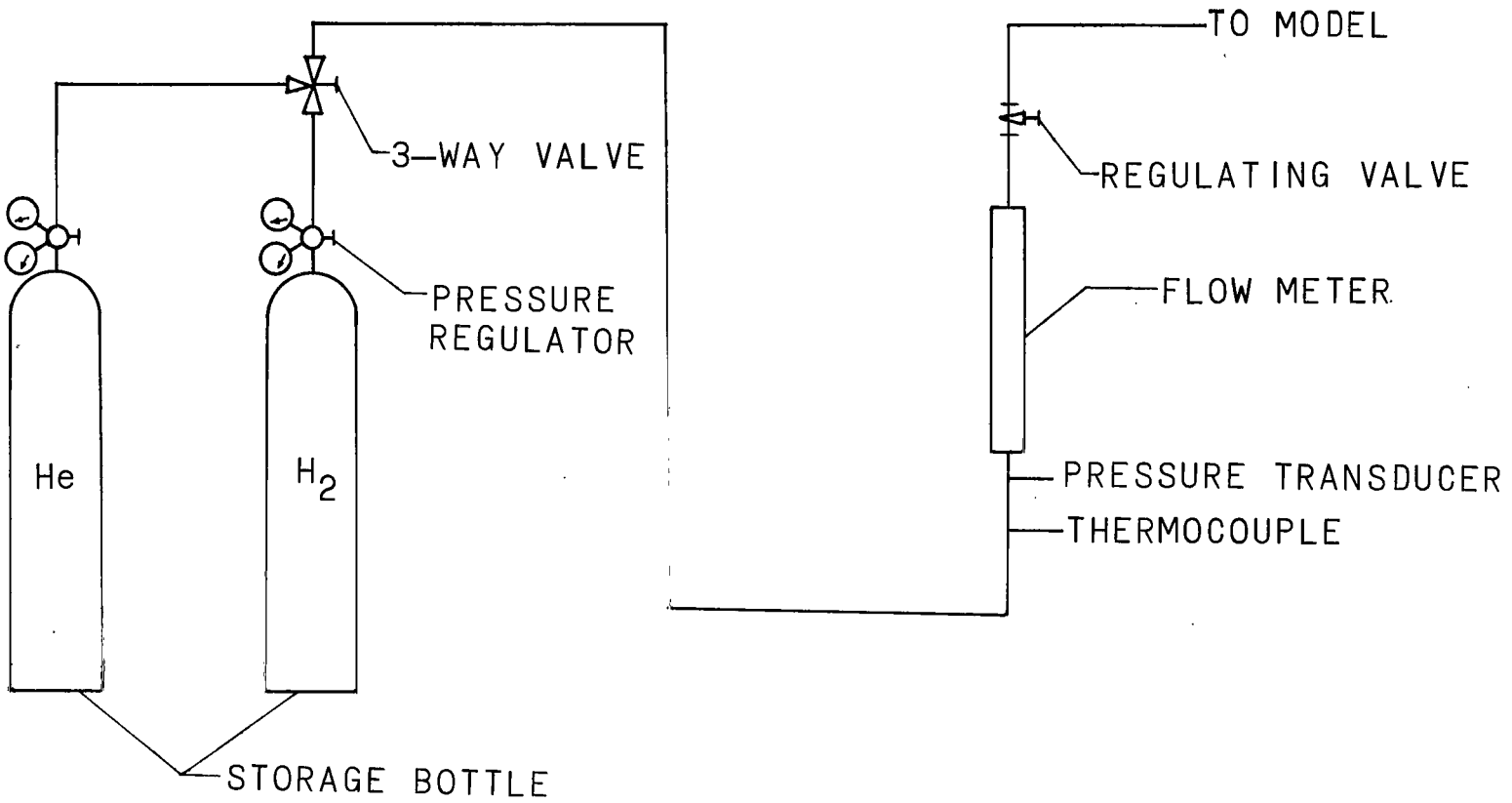

Figure 3.- Schematic sketch of cooling supply system (not to scale).

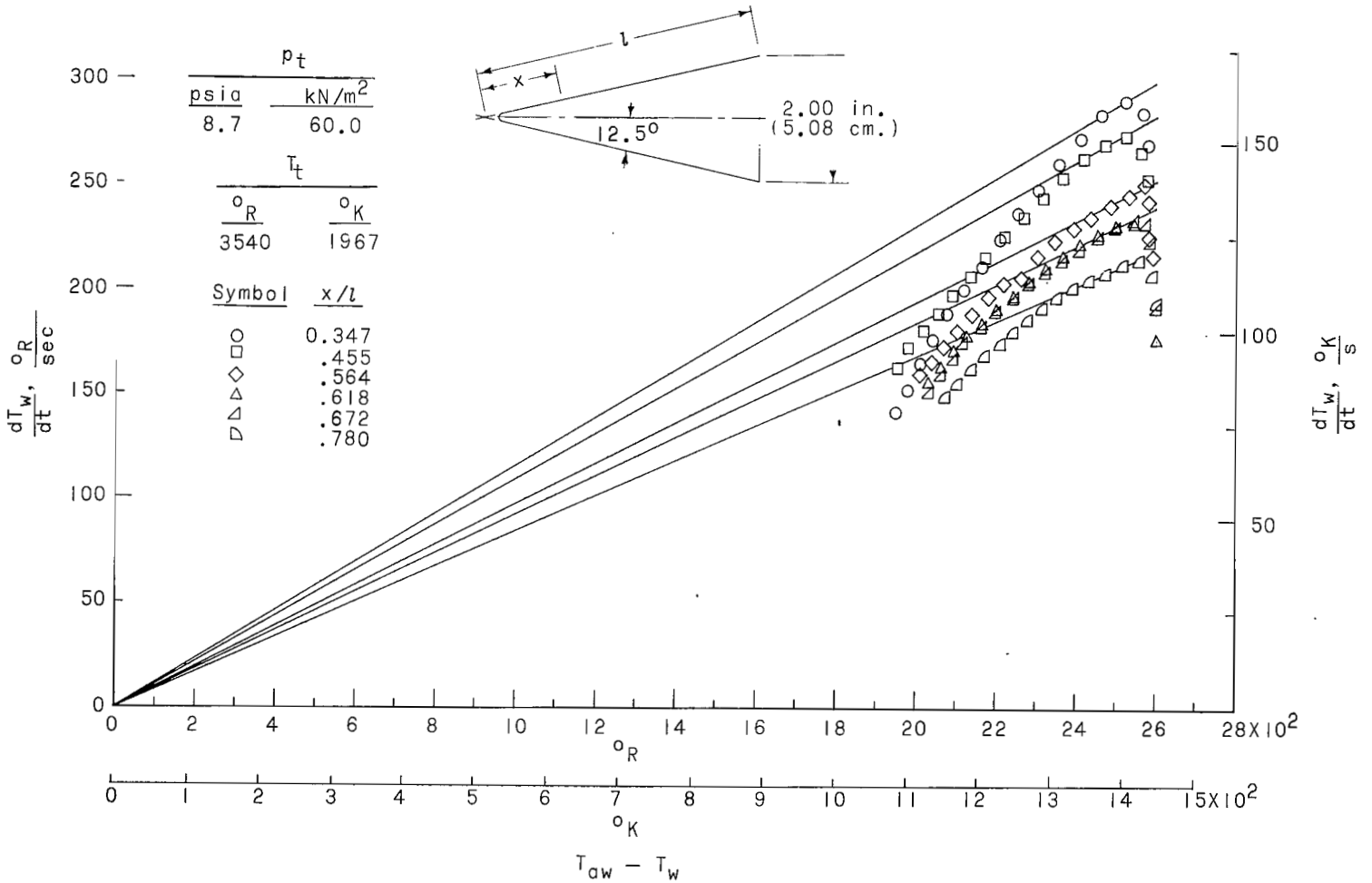

Figure 4.- Temperature-time slopes plotted against difference between adiabatic wall temperature and measured wall temperatures for various temperature measuring stations on uncooled heat-transfer surface.

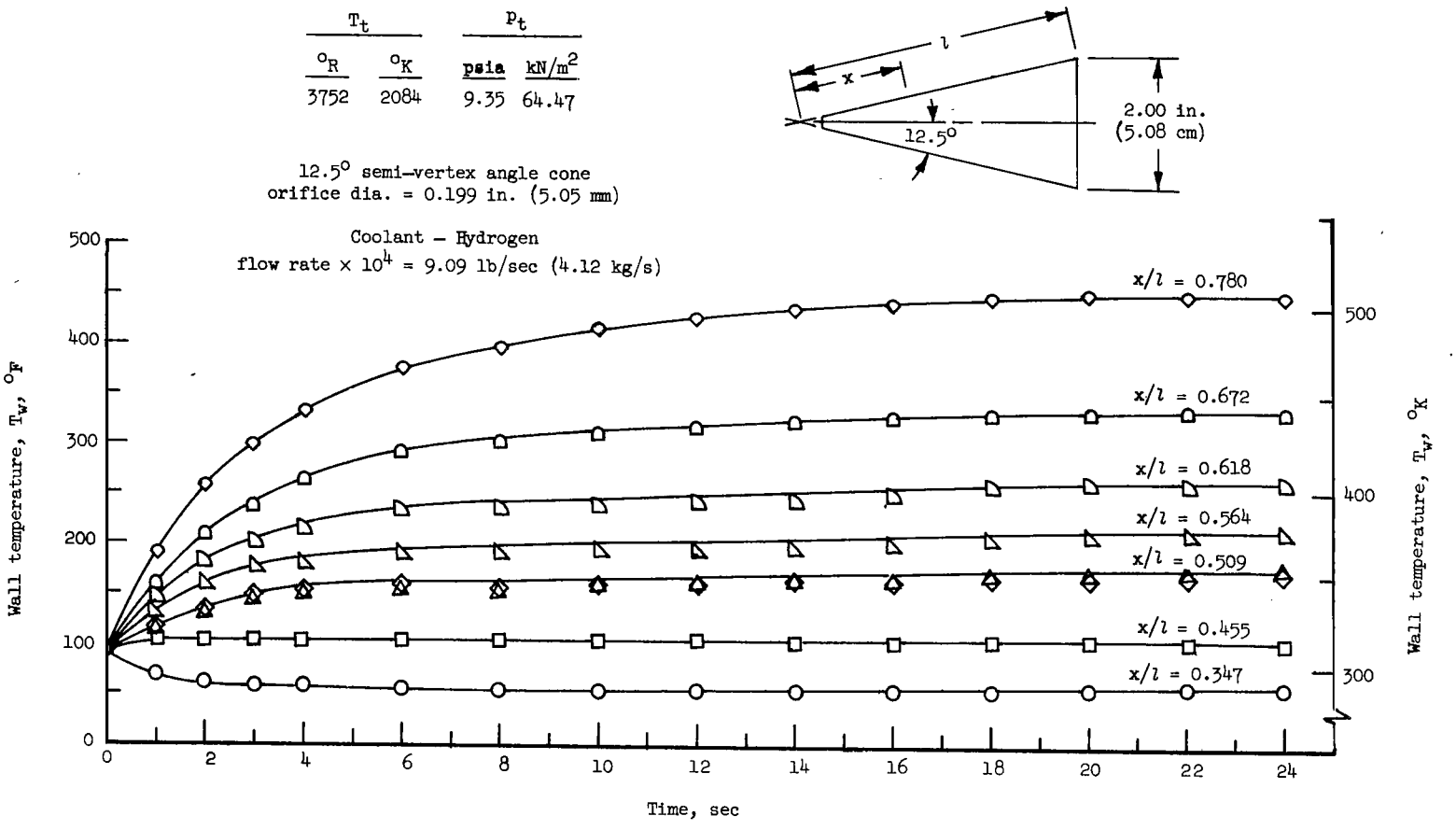

Figure 5.- Typical temperature histories of various measuring stations along heat-transfer surface with coolant flow.

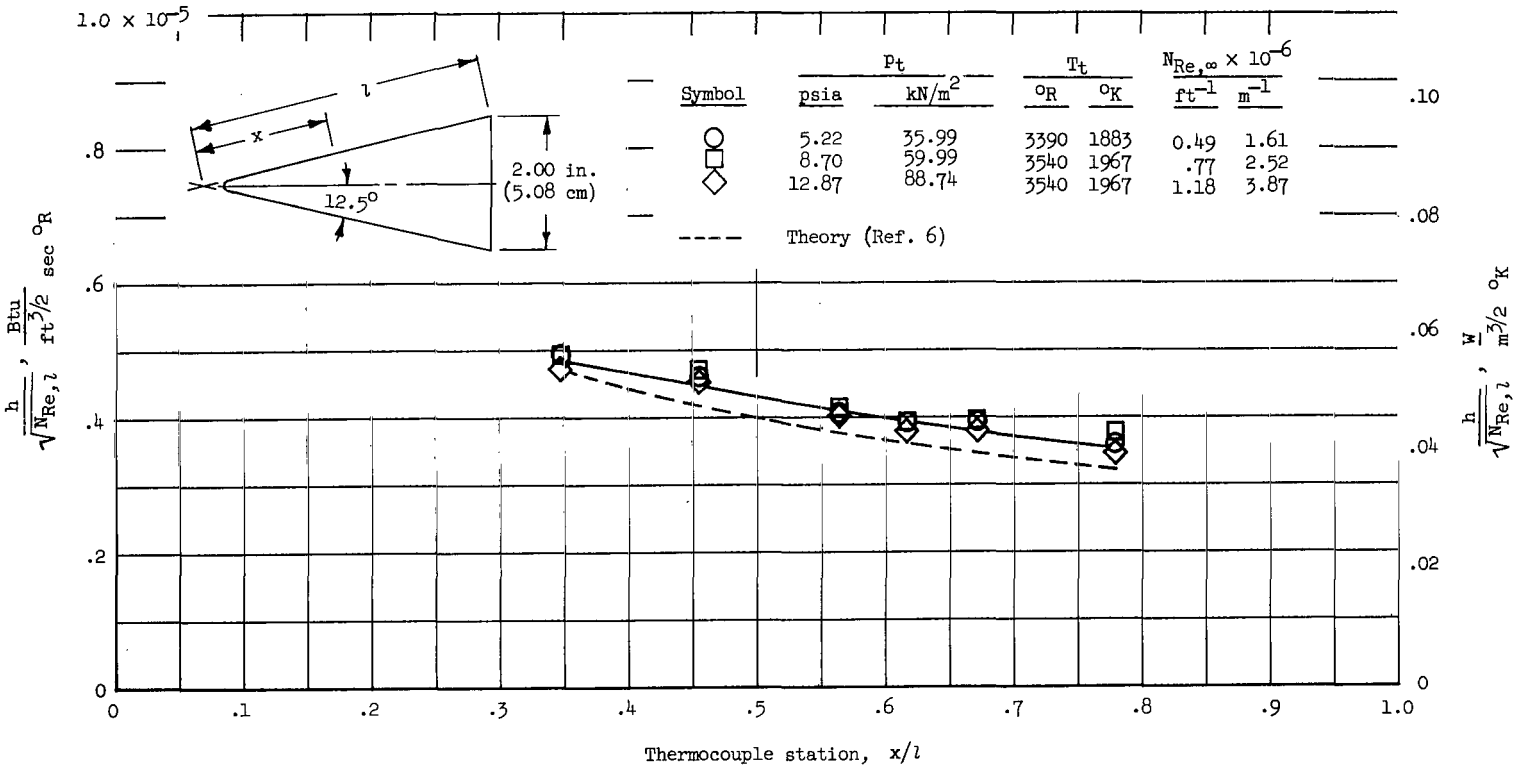

Figure 6.- Experimental and theoretical film heat-transfer coefficients for the uncooled heat-transfer surface.

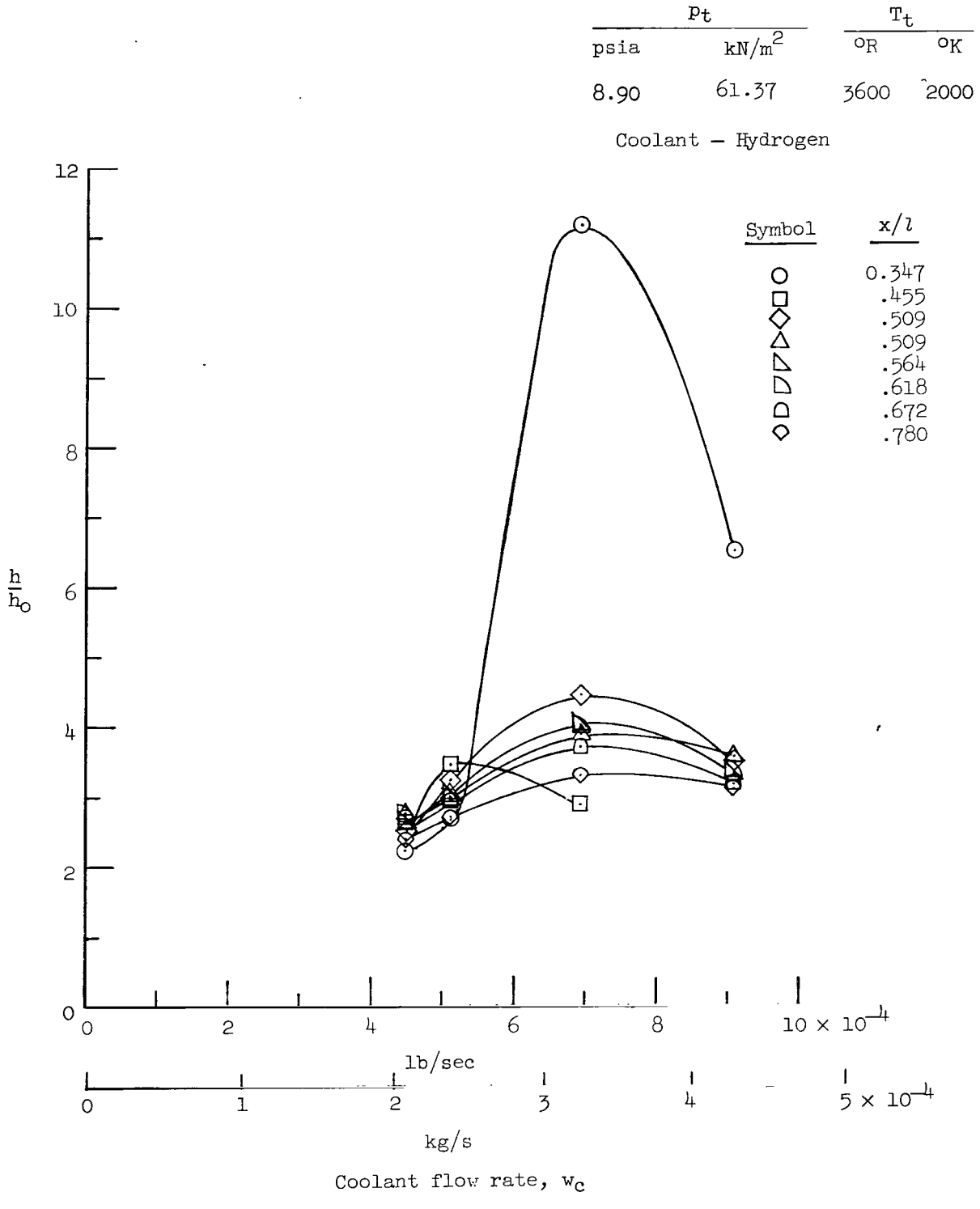

Figure 7.- Typical film heat-transfer coefficients for cooled heat-transfer surface at different coolant flow rates.

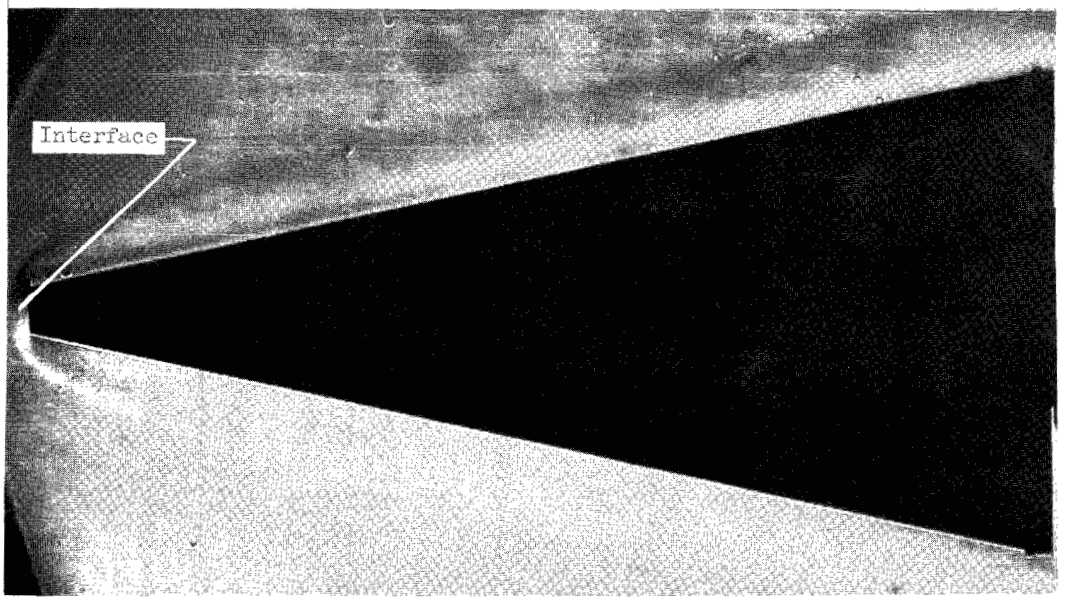

(a) Flow rate = 2.99×10^{-4} lb/sec (1.36×10^{-4} kg/s).

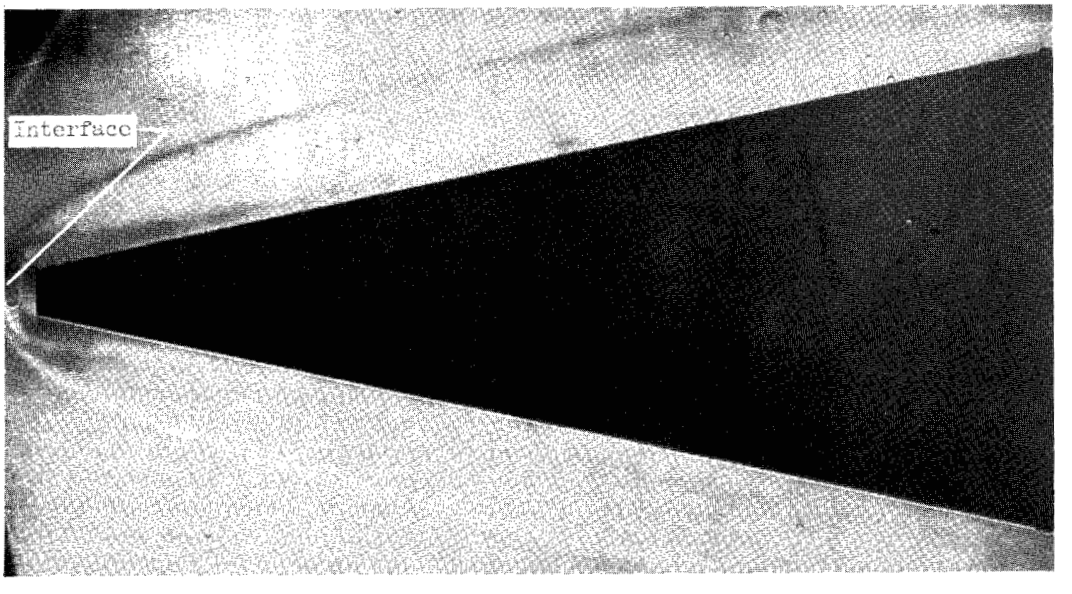

(b) Flow rate = 9.10×10^{-4} lb/sec (4.13×10^{-4} kg/s). L-64-4720

Figure 8.- Schlieren photographs illustrating changes in effective shape of model with different flow rates of hydrogen as a coolant at a model stagnation pressure of 5.8 psia (40.0 kN/m^2).

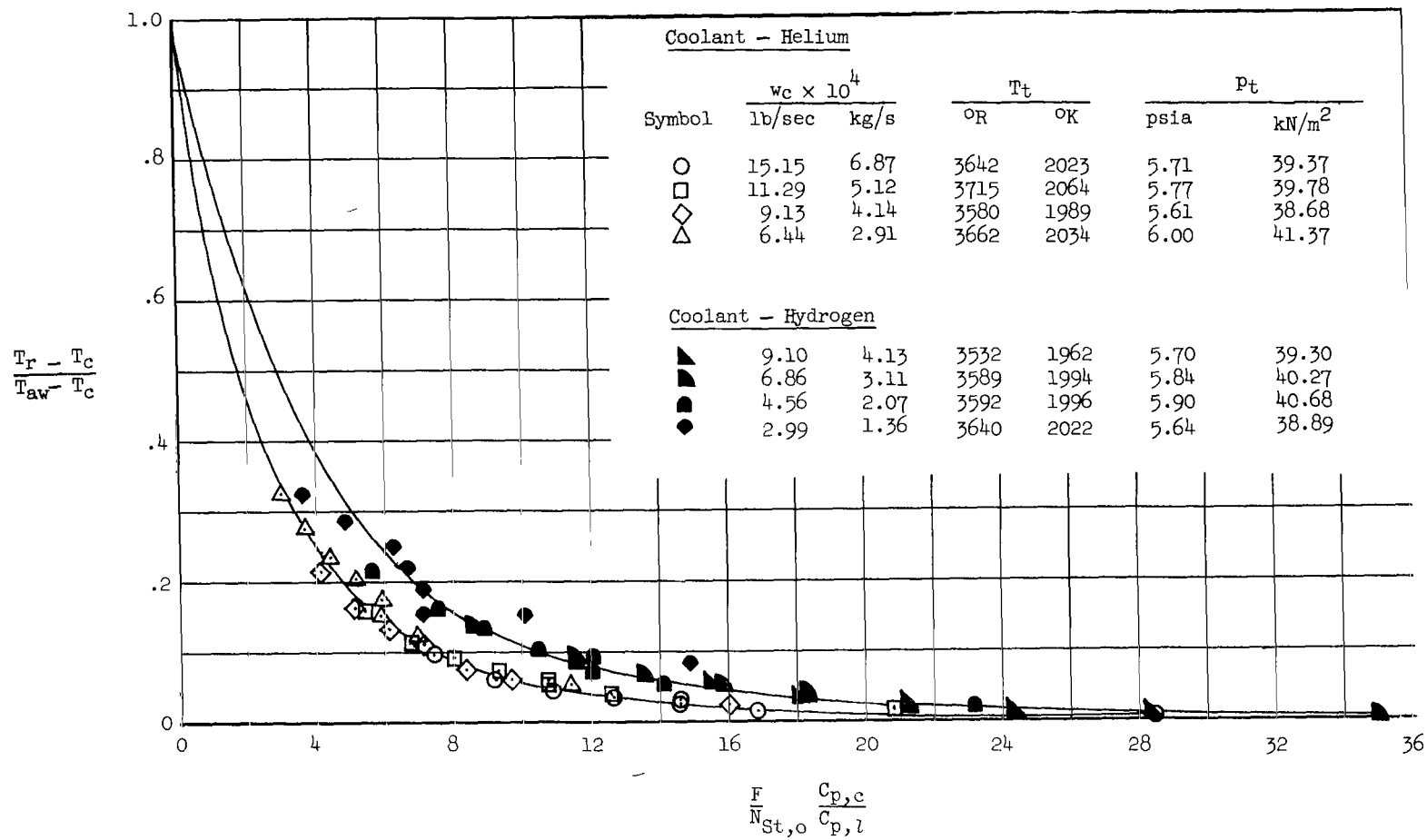

(a) p_t = 5.8 psia (40.0 kN/m^2); coolant orifice diameter = 0.199 in. (5.05 mm).

Figure 9.- Coolant effectiveness parameter plotted against correlating parameter.

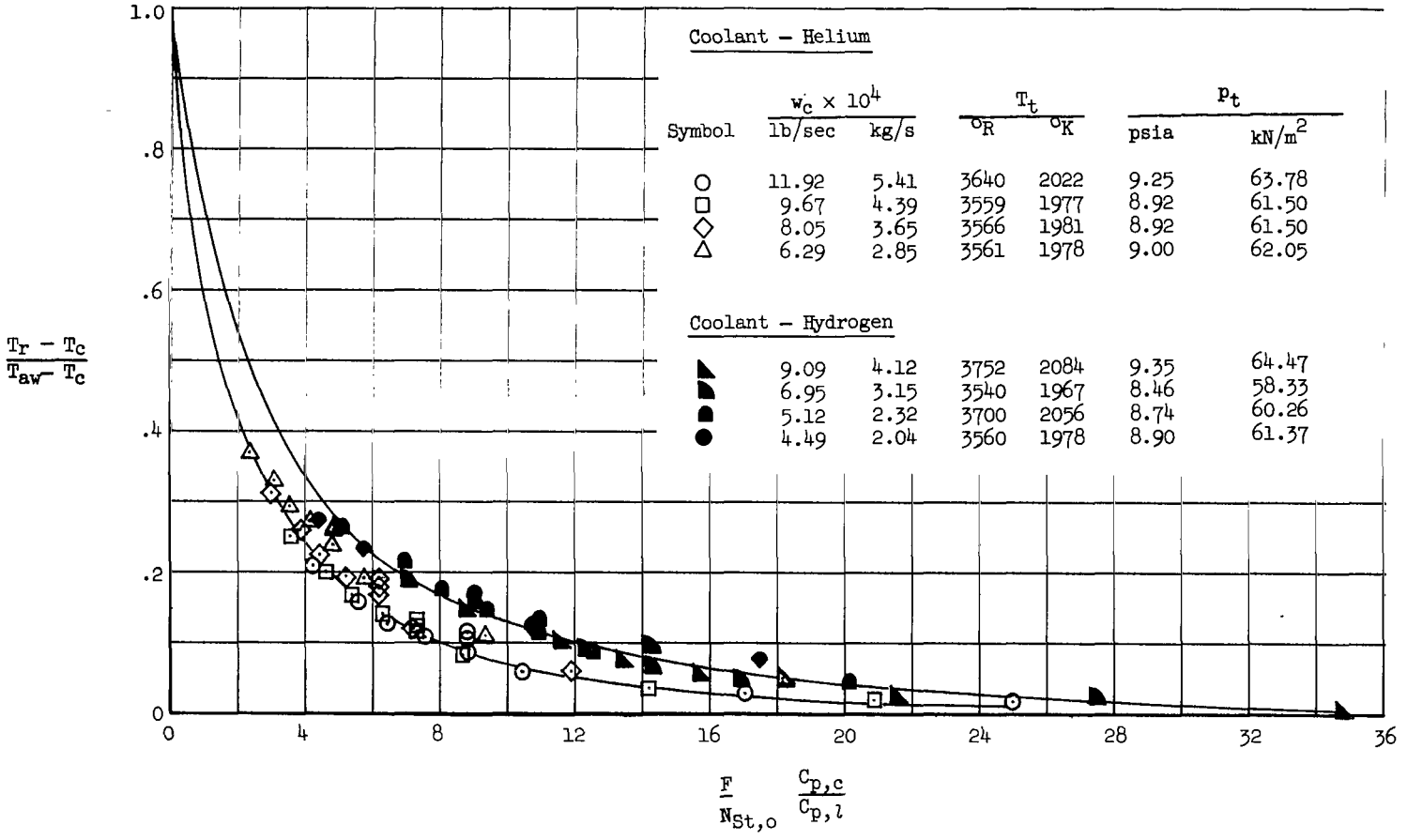

(b) p_t = 8.9 psia (61.4 kN/m²); coolant orifice diameter = 0.199 in. (5.05 mm).

Figure 9.- Continued.

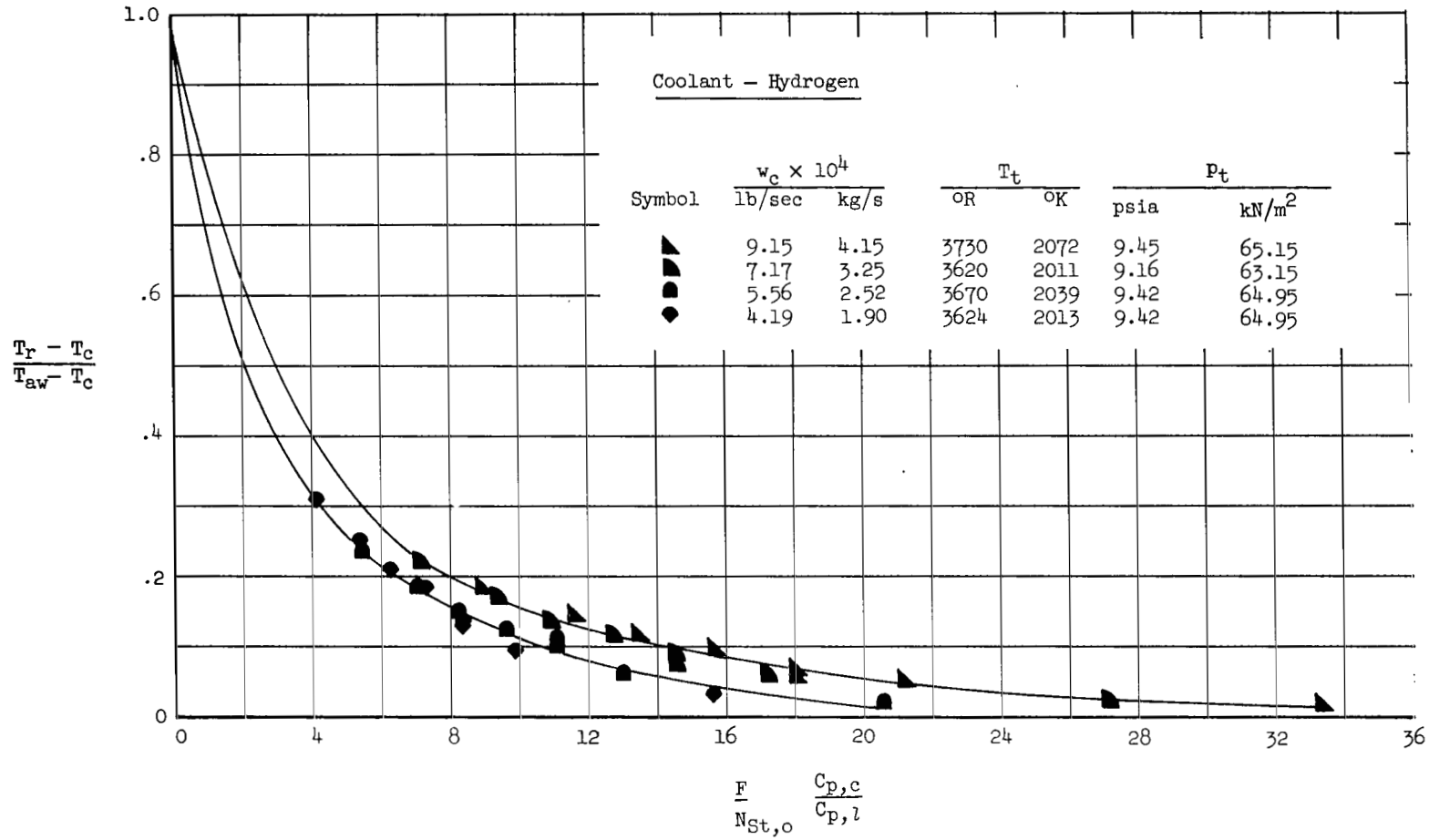

(c) p_t = 8.9 psia (61.4 kN/m²); coolant orifice diameter = 0.100 in. (2.54 mm).

Figure 9.- Continued.

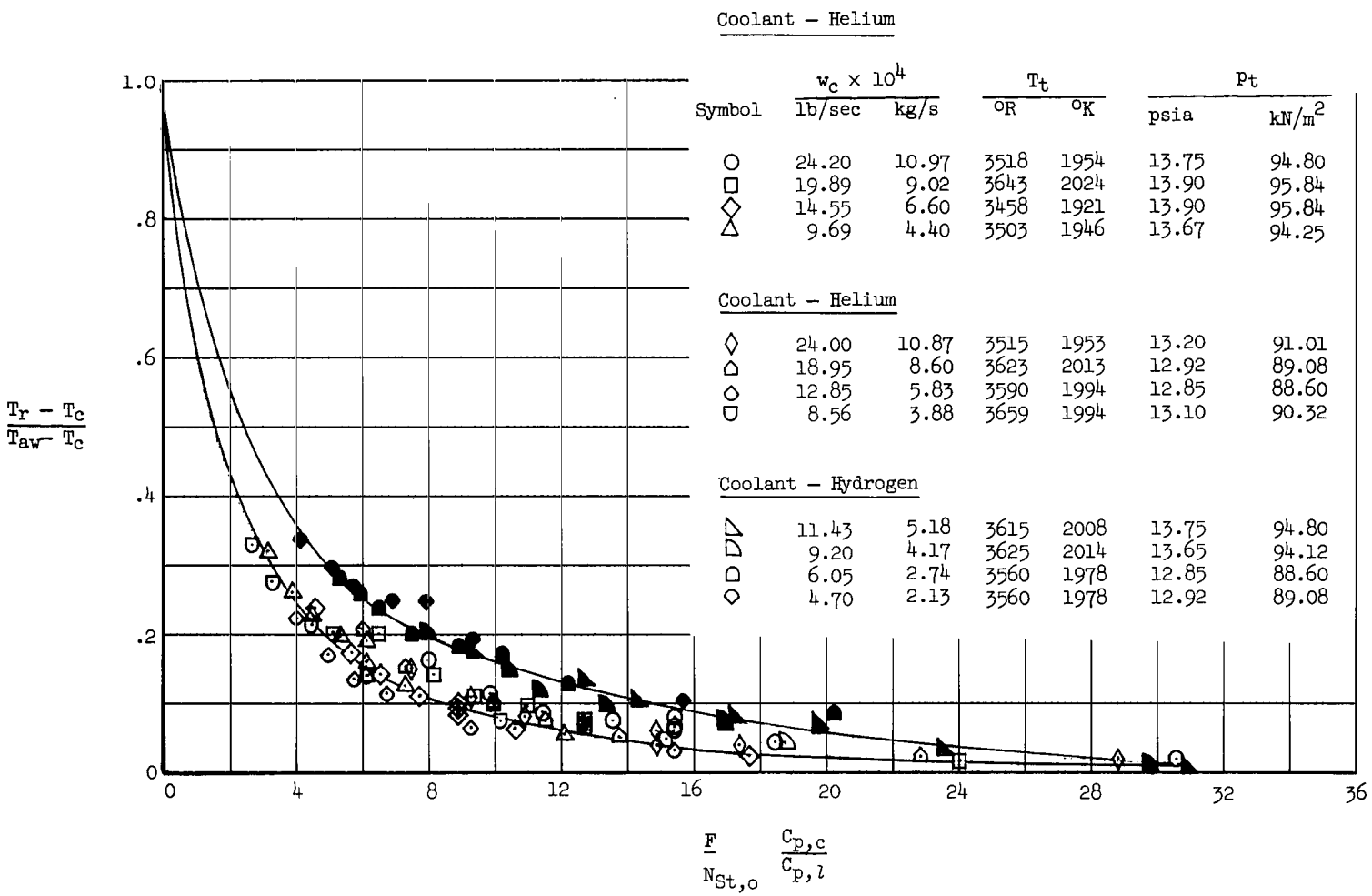

(d) p_t = 13.8 psia (95.2 kN/m^2); coolant orifice diameter = 0.199 in. (5.05 mm).

Figure 9.- Concluded.

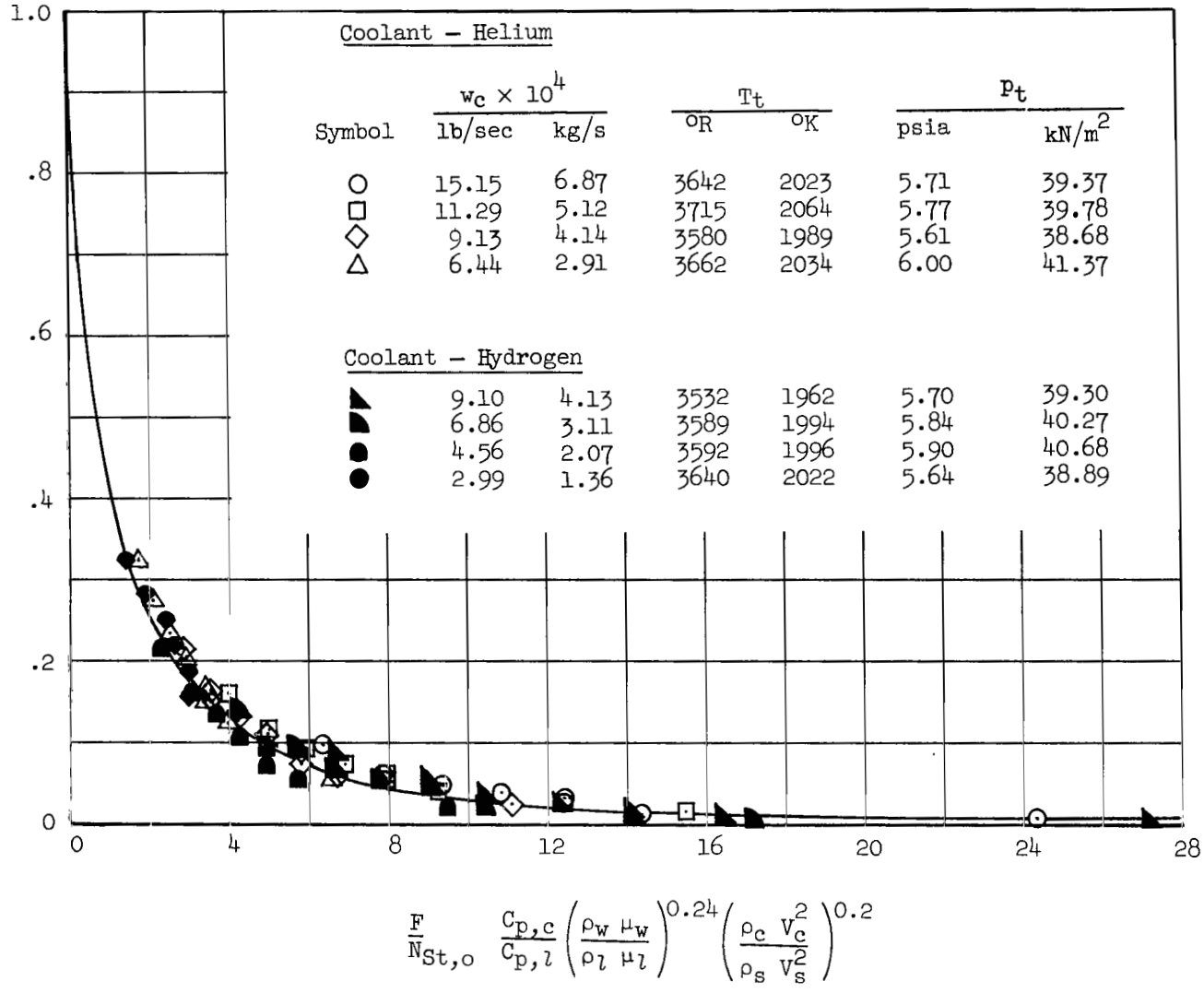

(a) p_t = 5.8 psia (40.0 kN/m²); coolant orifice diameter = 0.199 in. (5.05 mm).

Figure 10.- Variation of coolant effectiveness with modified correlating parameter for different test conditions and injection orifice sizes.

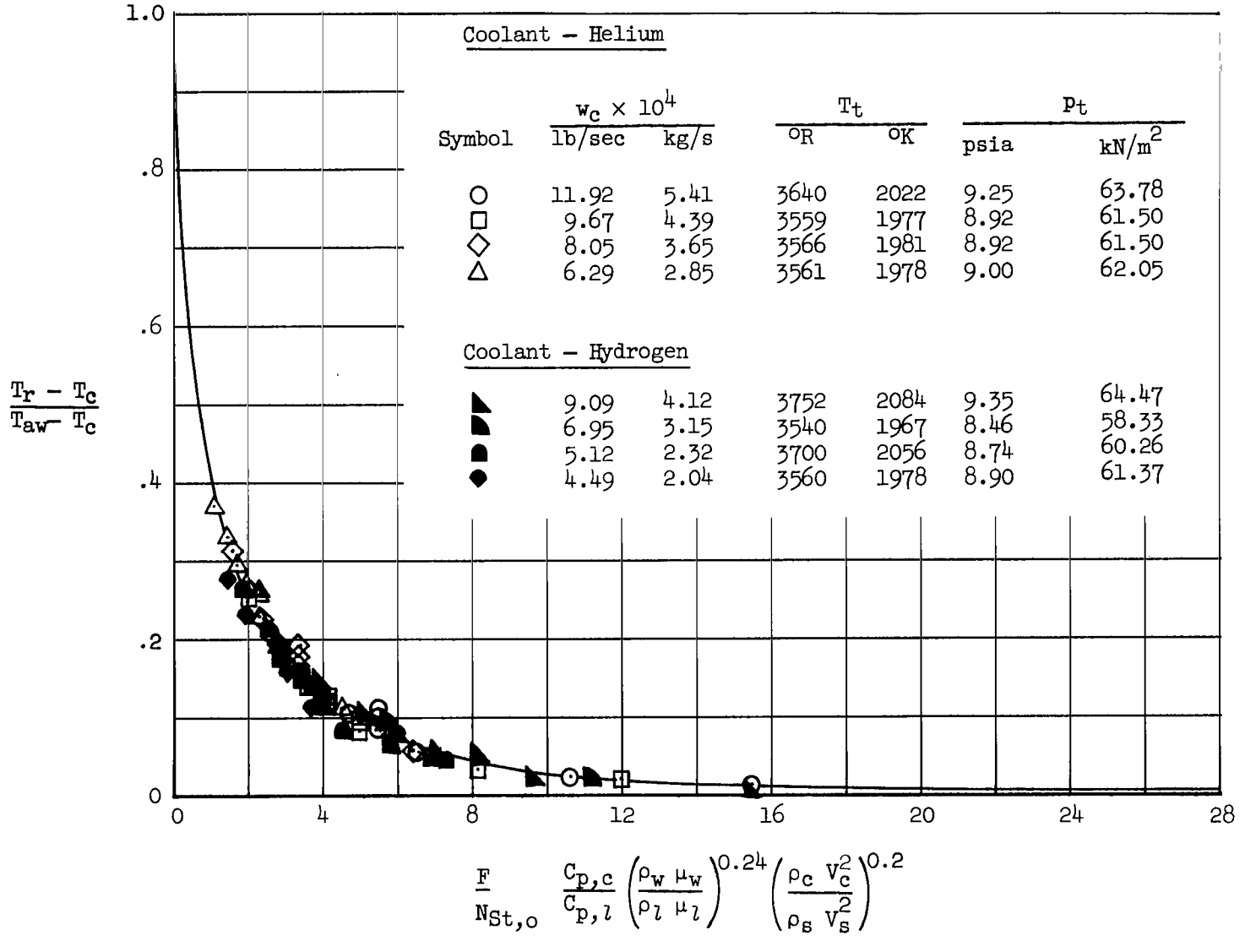

(b) p_t = 8.9 psia (61.4 kN/m²); coolant orifice diameter = 0.199 in. (5.05 mm).

Figure 10.- Continued.

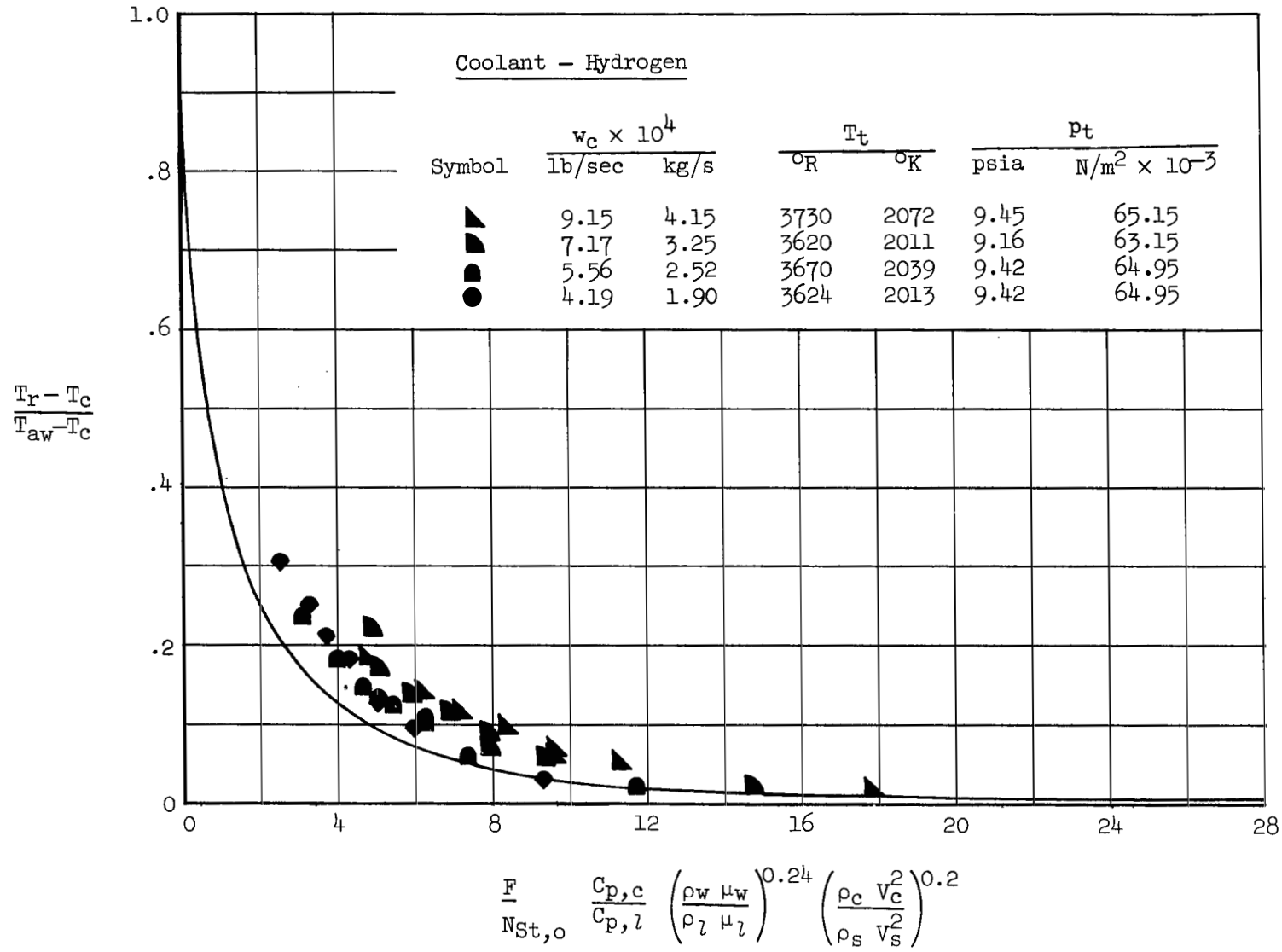

(c) p_t = 8.9 psia (61.4 kN/m²); coolant orifice diameter = 0.100 in. (2.54 mm).

Figure 10.- Continued.

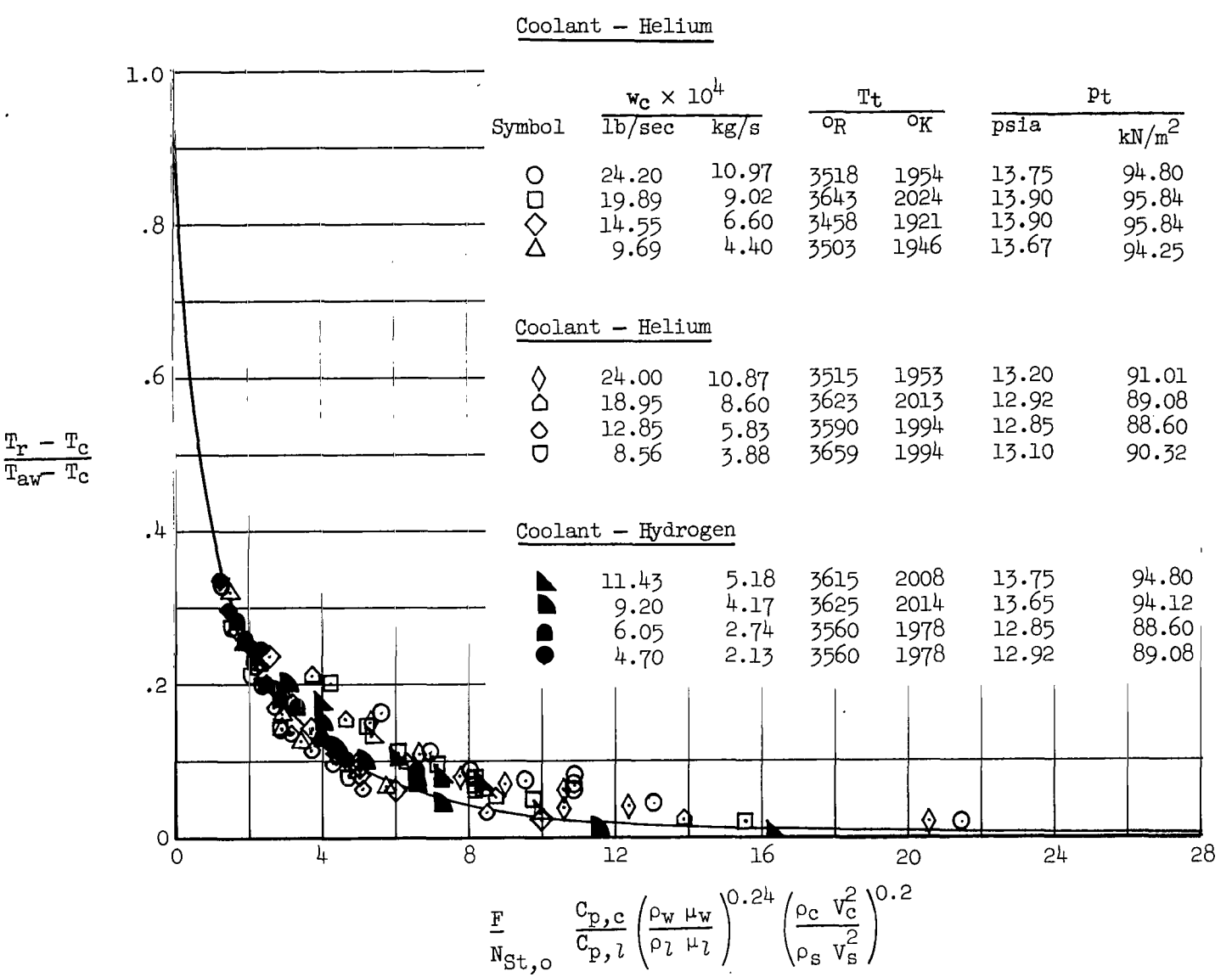

(d) p_t = 13.8 psia (95.2 kN/m²); coolant orifice diameter = 0.199 in. (5.05 mm).

Figure 10.- Concluded.

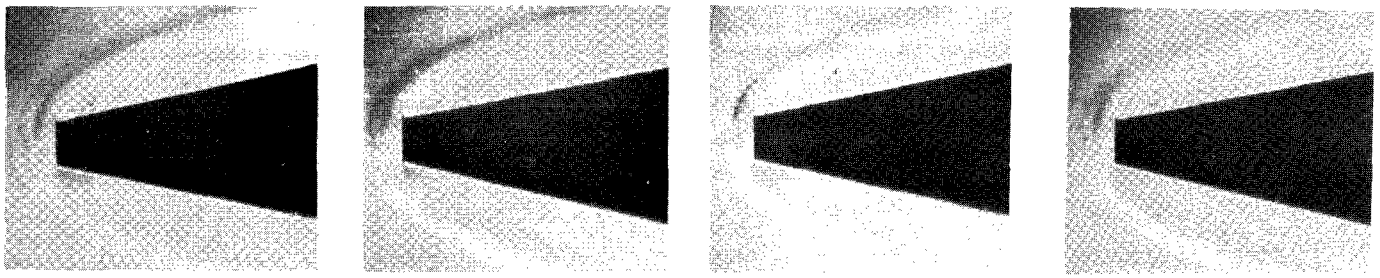

(a) t = 3 seconds. (b) t = 6 seconds. (c) t = 9 seconds. (d) t = 12 seconds.

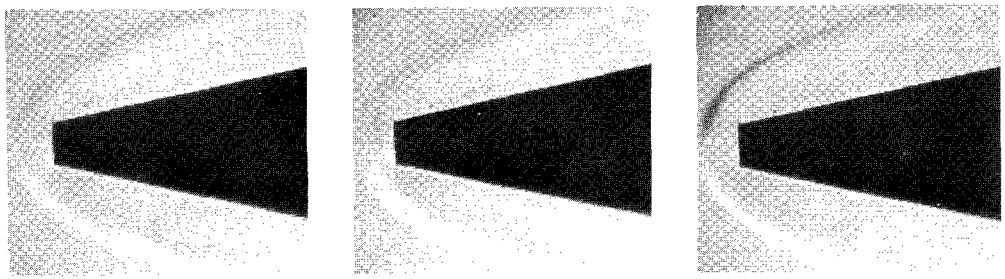

(e) t = 15 seconds. (f) t = 18 seconds. (g) t = 21 seconds. L-64-4721

Figure 11.- Schlieren photographs taken at various times during a test interval showing unsteadiness of bow shock wave. Coolant, helium; flow rate, 24.2×10^{-4} lb/sec (10.97×10^{4} kg/s); orifice diameter, 0.199 inch (5.05 mm); T_t = 3518° R (1954° K); p_t = 13.75 psia (94.80 kN/m^2).

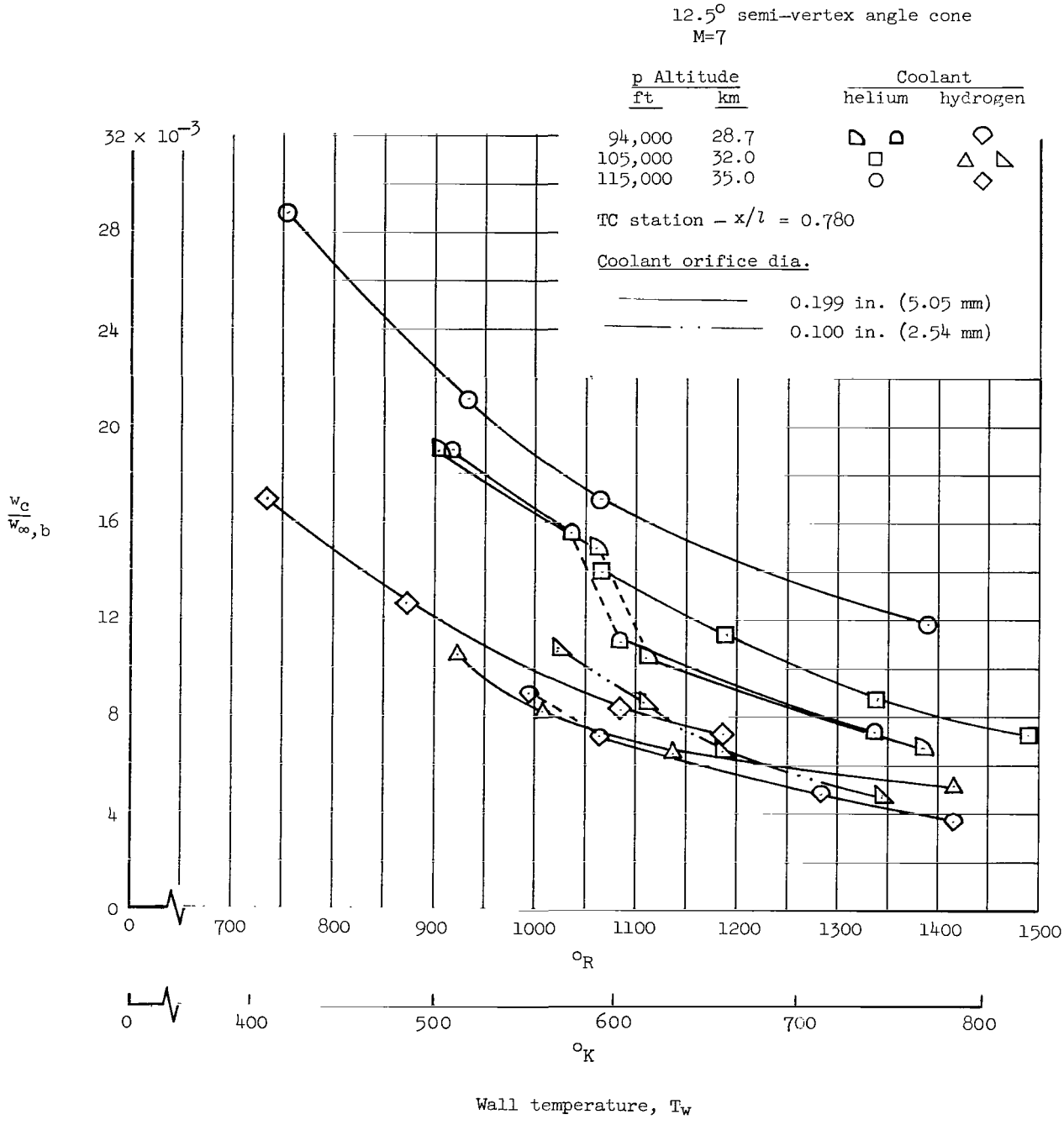

Figure 12.- Equilibrium wall temperatures of heat-transfer surface with coolant flow at various pressure altitudes at zero angle of attack.

2/11/25

"The aeronautical and space activities of the United States shall be conducted so as to contribute . . . to the expansion of human knowledge of phenomena in the atmosphere and space. The Administration shall provide for the widest practicable and appropriate dissemination of information concerning its activities and the results thereof."

—NATIONAL AERONAUTICS AND SPACE ACT OF 1958

NASA SCIENTIFIC AND TECHNICAL PUBLICATIONS

TECHNICAL REPORTS: Scientific and technical information considered important, complete, and a lasting contribution to existing knowledge.

TECHNICAL NOTES: Information less broad in scope but nevertheless of importance as a contribution to existing knowledge.

TECHNICAL MEMORANDUMS: Information receiving limited distribution because of preliminary data, security classification, or other reasons.

CONTRACTOR REPORTS: Technical information generated in connection with a NASA contract or grant and released under NASA auspices.

TECHNICAL TRANSLATIONS: Information published in a foreign language considered to merit NASA distribution in English.

TECHNICAL REPRINTS: Information derived from NASA activities and initially published in the form of journal articles.

SPECIAL PUBLICATIONS: Information derived from or of value to NASA activities but not necessarily reporting the results of individual NASA-programmed scientific efforts. Publications include conference proceedings, monographs, data compilations, handbooks, sourcebooks, and special bibliographies.

Details on the availability of these publications may be obtained from:

SCIENTIFIC AND TECHNICAL INFORMATION DIVISION

NATIONAL AERONAUTICS AND SPACE ADMINISTRATION

Washington, D.C. 20546